A Simple, Fast, and Robust Open-Phase Fault Detection Technique for Six-Phase Induction Motor Drives

Mario J. Duran, Ignacio Gonzalez-Prieto, Natalia Rios-Garcia, and Federico Barrero, *Senior Member, IEEE*

***Abstract*—Fault tolerance is much appreciated at industry in applications with high-reliability requirements. Due to their inherent fault-tolerant capability against open-phase faults (OPFs), drives with multiple three-phase windings are ideal candidates in such applications and for this reason many efforts have been devoted to the development of different fault-tolerant control strategies. Fault detection is, however, a previous and mandatory stage in the creation of fault-tolerant drives, and the study of specific OPF detection methods for six-phase drives is still scarce. Taking advantage of the secondary currents (so called *x*-*y* currents) that are unique in multiphase machines, this study proposes new fault indices that detect and locate the OPFs without additional hardware. The method proves to be simple and independent of the operating point, control technique, and drive parameters. Comparative experimental results confirm the capability of the proposed method to achieve fast detection times with good robustness.**

***Index Terms*—Fault detection, multiphase induction motor drives, open-phase faults (OPFs).**

I. Introduction

BEING favored by the economy of scales and a proven technology, three-phase machines dominate the market in variable-speed drive applications. Nevertheless, recent efforts have been devoted to highlight the advantages of multiphase machines and to find a niche of applications where they can compete with the three-phase standard [1]–[3]. Since the fault tolerance provided by the redundant phases is a unique feature of multiphase machines, industry has initially focused on high-reliability applications, such as aerospace, traction, or wind energy systems to include machines with multiple three-phase windings [4]–[8]. With these applications in mind, many recent works have been focused on the development of high-performance fault-tolerant control schemes for induction machines (IMs) and permanent magnet synchronous machines (PMSMs) [7]–[18].

Manuscript received November 16, 2016; revised January 19, 2017; accepted February 7, 2017. Date of publication February 17, 2017; date of current version October 6, 2017. This work was supported by the Spanish Ministry of Science and Innovation under Project ENE2014-52536-C2-1-R. Recommended for publication by Associate Editor L. Dalessandro.

M. J. Duran, I. Gonzalez-Prieto, and N. Rios-Garcia are with the Department of Electrical Engineering, University of Malaga, Malaga 29071, Spain (e-mail: mjduran@uma.es; ignaciogp87@gmail.com; nrg@uma.es).

F. Barrero is with the Department of Electronic Engineering, University of Seville, Seville 41092, Spain (e-mail: fbarrero@us.es).

Color versions of one or more of the figures in this paper are available online at http://ieeexplore.ieee.org.

Digital Object Identifier 10.1109/TPEL.2017.2670924

The first step in this direction was the modification of standard field-oriented control (FOC) to obtain a ripple-free postfault operation [7]–[14], but the widely used direct torque control has also found its fault-tolerant version recently [15]. Apart from these two mainstream control strategies, some other modern control techniques, such as the model-based predictive control (MPC) and sliding mode control have also modified the healthy schemes to operate after the fault occurrence [16]–[18]. Regardless of the control approach, an open-phase fault (OPF) has been considered in [7]–[18] and the fault-tolerant control is performed using the remaining healthy phases. Since the focus in these works has been placed on control issues, the aforementioned works have either directly omitted the transition from pre- to postfault situations [7]–[14], [18] or have considered an arbitrary fault detection delay [15]–[17]. It is, however, clear that the postfault control can only be activated after the fault has been detected, and the investigation on OPF detection methods for multiphase systems is still scarce.

Fault diagnosis in electrical machines can be used to detect incipient faults, and this leads to fast unscheduled corrective maintenance, short downtimes, and elimination of harmful side effects [19]. In such cases, many different fault types should be taken into account (e.g., broken rotor bars or interturn faults, to name a few) and relatively long detection times can be permitted [20]. On the other hand, if the aim of the fault detection is to apply any of the fault-tolerant techniques detailed in [7]–[18], the fault detection should be concentrated in OPFs [21] and detection times should be as short as possible (typically less than one fundamental period). Since the fault detection method is combined with a high-performance postfault control, it should in principle possess the following requirements:

- R1) use of noninvasive techniques and lack of additional hardware (e.g., voltage measurements [22]);
- R2) obtain short detection times (less than a fundamental period) that avoid torque ripple, vibrations, and overcurrents;
- R3) avoid complex approaches with a high implementation effort;
- R4) lack of operating condition dependence (load dependence and sensitivity to transients);
- R5) lack of dependence on the machine parameter and/or control strategy.

A method for seven-phase IMs that uses the reference voltage of the secondary components in an FOC strategy is proposed in [23], but it is focused on stator resistance dissymmetry and depends on the control strategy. Five-phase PMSMs are considered in [24] and [25], but also aiming to detect incipient interturn short-circuit faults and using additional voltage measurements. A fault diagnosis proposal for five-phase PMSMs in [26] uses an observed-based approach with an index based on the cross correlation of the estimated and measured currents. Since the method is model-based, the estimations imply some additional calculations that require the knowledge of the motor parameters (violating requirements *R3* and *R5*), which are known to vary with the operating point (due to thermal effects, magnetic saturation, and skin effect, to name some of the typical causes for the parameters mismatch). A slightly different approach is adopted in [27] together with an MPC strategy, but the approach is again observer-based, and, consequently, it suffers from similar limitations as in [26]. A fault-detection system based on the rms value of the stator currents is suggested in [28] for a symmetrical six-phase IM, but the fault detection index is not normalized and the detection delay is higher than a fundamental cycle (failing to fulfill requirements *R2* and *R4*).

The aforementioned requirements are generally fulfilled by methods that follow the commonly referred as Park vector approach [19], [20]. Since most of these methods are designed on a per-phase basis, they can be in principle extended to other machines regardless of the number of phases. This is the case of [29]–[32], which were identified in [19] and [20] as benchmark approaches for the OPF detection. In [29]–[32], the requirement *R4* is fulfilled using normalized fault detection indices. While the normalization in [31] and [32] is based on the average absolute values of the motor phase currents, the modulus of the Park vector is employed in [29] and [30]. With different performances in several figures of merit, the methods proposed in [29]–[32] show effectiveness, good detection speed, robustness, and low implementation effort. A similar approach can be found in [33], but using a normalization that includes the additional subspace existing in five-phase machines. The methods in [34]–[36] also follow the main trend of detecting the OPF identifying the pattern of distortion in the $d-q$ currents caused by the fault. Although the methods in [31] and [32] can be extended with small modifications to multiphase machines, neither these methods nor the multiphase ones found in [23], [26]–[28], and [33]–[36] take advantage of the specific components (termed *x-y* in what follows) that appear in a multiphase system. Compared to phase currents, the *x-y* currents present some properties that make them good candidates to be used as fault indices:

1) the *x-y* components are constant (null) in healthy operation, whereas phase currents are sinewaves;
2) the *x-y* components are not related to the torque production (in distributed-winding machines), and, consequently, they are inherently independent of the drive dynamics.

Following the idea of involving these secondary current components to improve the fault detection in six-phase drives, this study specifically presents the following contributions:

1) the fault detection method in [29] and [30] is extended to six-phase drives;
2) a new fault detection method based on normalized *x-y* currents is presented;
3) the proposed method based on the vector space decomposition (VSD) approach is experimentally compared to previous techniques [29], [30] based in the Park approach to show the superior characteristics.

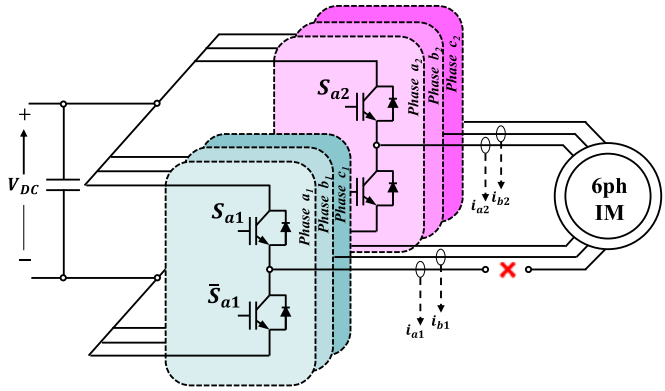

Fig. 1. Scheme of the six-phase induction motor drive in OPF operation.

This paper is structured as follows. Section II reviews the background on six-phase IM drives in OPF operation. Section III discusses some generalities about the OPF detection, extends the method in [29] and [30] to the six-phase case, and points out the main limitations of the phase-current-based approach. Section IV presents the proposed VSD-based fault detection (VSDFD) method and enumerates its potential advantages. Section V describes the experimental rig and shows obtained results, and Section VI finally summarizes the main conclusions.

II. Generalities of Six-Phase Induction Motor Drives in OPF Operation

The drive under study consists of an asymmetrical six-phase IM supplied from two three-phase voltage-source converters (VSCs) that are connected to a single dc-link (see Fig. 1). The IM has two sets of three-phase windings ($a_1b_1c_1$ and $a_2b_2c_2$) that are spatially shifted 30 electrical degrees with isolated neutral points. The converters (VSC_1 and VSC_2) are two-level Insulated Gate Bipolar Transistor-based type, each one connected to the sets 1 and 2 of three-phase windings, respectively.

As in three-phase drives, it is convenient for control purposes to use the VSD in order to obtain flux- and torque-related *d-q* currents. However, since the system is six-dimensional, the generalized Clarke transformation

$$[T]=\frac{1}{\sqrt{3}}\begin{bmatrix}1 & -1/2 & -1/2 & \sqrt{3}/2 & -\sqrt{3}/2 & 0\\ 0 & \sqrt{3}/2 & -\sqrt{3}/2 & 1/2 & 1/2 & -1\\ 1 & -1/2 & -1/2 & -\sqrt{3}/2 & \sqrt{3}/2 & 0\\ 0 & -\sqrt{3}/2 & \sqrt{3}/2 & 1/2 & 1/2 & -1\\ 1 & 1 & 1 & 0 & 0 & 0\\ 0 & 0 & 0 & 1 & 1 & 1\end{bmatrix}$$

$$[i_{\alpha s}i_{\beta s}i_{xs}i_{ys}i_{0+}i_{0-}]^T=[T]\cdot[i_{a1}i_{b1}i_{c1}i_{a2}i_{b2}i_{c2}]^T \quad (1)$$

includes new *x*-*y* current components in addition to the standard $\alpha-\beta$ and zero-sequence components (0_+–0_-). The VSD was originally presented in [37] and showed that the variables after the decomposition can be grouped in $\alpha-\beta$ and $x-y$ vectors that form orthogonal subspaces (also termed planes), and this mathematical characteristic implies that the new $x-y$ components can be controlled independently of the $\alpha-\beta$ components. The $\alpha-\beta$ subspace plays a similar role as in three-phase drives, serving at the control stage to regulate the flux and torque using *d*- and *q*-components, respectively, once the Park transformation is performed

$$[D] = \begin{bmatrix} \cos\theta_s & \sin\theta_s \\ -\sin\theta_s & \cos\theta_s \end{bmatrix}$$
$$[i_{ds} i_{qs}]^T = [D] \cdot [i_{\alpha s} i_{\beta s}]^T$$
$$\theta_s = \int \left(p \cdot \omega_m - \frac{i_q^*}{T_r \cdot i_d^*} \right) \cdot dt \tag{2}$$

where θ_s is the angle of the rotating reference frame that is obtained from the measured speed ω_m and the estimated slip, being p the number of pole pairs and T_r the rotor time constant.

On the other hand 0_+-0_- current components will be omitted further on from the analysis since they do not flow due to the two isolated neutrals configuration. The major difference compared to three-phase machines is the new *x*-*y* subspace, and for this reason, it has been the focus of some innovations [7], [38], [39] that cannot be done in three-phase drives where these components simply do not exist. If the machine has distributed windings, these components become circulating stator currents that do not contribute to the torque or flux production.

The equations of the six-phase machine in VSD variables can, thus, be expressed as [10]:

$$v_{\alpha s} = \left(R_s + L_s \frac{d}{dt} \right) i_{\alpha s} + M \frac{d i_{\alpha r}}{dt}$$
$$v_{\beta s} = \left(R_s + L_s \frac{d}{dt} \right) i_{\beta s} + M \frac{d i_{\beta r}}{dt}$$
$$v_{xs} = \left(R_s + L_{ls} \frac{d}{dt} \right) i_{xs}$$
$$v_{ys} = \left(R_s + L_{ls} \frac{d}{dt} \right) i_{ys}$$
$$0 = \left(R_r + L_r \frac{d}{dt} \right) i_{\alpha r} + M \frac{d i_{\alpha s}}{dt} + \omega_r L_r i_{\beta r} + \omega_r M i_{\beta s}$$
$$0 = \left(R_r + L_r \frac{d}{dt} \right) i_{\beta r} + M \frac{d i_{\beta s}}{dt} - \omega_r L_r i_{\alpha r} - \omega_r M i_{\alpha s}$$
$$T_e = pM \left(i_{\beta r} i_{\alpha s} - i_{\alpha r} i_{\beta s} \right) \tag{3}$$

where $L_s = L_{ls} + 3L_m$, $L_r = L_{lr} + 3L_m$, $M = 3L_m$ and ω_r is the rotor electrical speed ($\omega_r = p\omega_m$). Subscripts *s* and *r* denote stator and rotor variables, respectively.

When an OPF occurs, the model of the machine from (3) is still valid, but the loss of one degree of freedom implies that the VSD variables are no longer independent. Assuming in what follows and without lack of generality that the fault affects phase

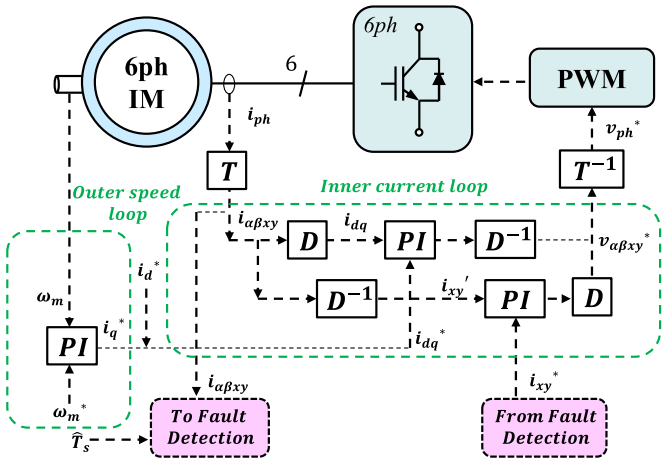

Fig. 2. Control scheme in prefault situation (see Fig. 4 to link with the fault detection scheme).

a_1 in single OPF scenario, it follows from (1) that the postfault restriction is

$$i_{xs} = -i_{\alpha s}. \tag{4}$$

The *y*-current is still independent and its reference value is taken according to a minimum loss ($i_{ys}^* = 0$) or minimum derating ($i_{ys}^* = -i_{\beta s}$) criterion [3].

As far as the control is concerned, the most widespread approach is the FOC with some modifications that take into account the nonzero value of the *x*-*y* currents [9]–[11], [23]. The control scheme follows a nested approach with an outer speed loop that provides the *q*-current reference and inner current loops that provide the voltage references for the modulation stage (either carrier-based or space vector pulse width modulation), as shown in Fig. 2. While the speed and *d*-*q* current controllers use standard proportional-integral (PI) controllers, the *x*-*y* current controllers are PI in normal operation (see Fig. 2) and might need to become resonant after the fault occurs in order to track the nonzero references from the fault detection stage (see Fig. 4 in Section IV for further details).

In relation to the fault detection method that will be introduced in Section IV, the most remarkable feature of the six-phase machine is the appearance of the *x*-*y* subspace. Specifically, it is to be noted that 1) the *x*-*y* currents do not need to be specifically calculated since they are already available from the control stage (see Fig. 2), 2) the *x*-*y* components are null before the fault and nonnull after the fault occurrence, and 3) the torque in (3) only involves the $\alpha-\beta$ subspace. This suggests the adequacy of using fault detection indices based on VSD *x*-*y* currents.

III. Background on Open-Phase Fault Detection and Extension of Three-Phase Methods

The open-phase fault detection methods essentially aim to know as soon as possible if a phase has been disconnected from the motor in order to apply any of the postfault strategies detailed in [7]–[18], to name a few. Since the steady-state phase currents are sinewaves of variable amplitude and frequency in

variable-speed drives, all phase currents naturally become zero twice in a fundamental period.

Furthermore, multiple crossings at zero can be found in industrial applications due to the current ripple. It is, therefore, necessary to distinguish between the null current that is obtained after the OPF occurrence and the multiple zero crossings that happen in normal operation. In spite of the claims that can be found in some works, a fault detection time in the order of the microseconds can only be obtained in simulation studies. To aggravate the achievement of a correct fault detection, measurement errors must be taken into account and transients may also cause zero crossings and lead to false alarms [19], [20]. All that said there is still room for a quick fault detection that should be done in less than a quarter of the fundamental period.

Since the fault detection cannot be performed using instantaneous values due to the possibility to confuse the OPF with a zero crossing, a normal approach is to average phase currents over a fundamental period T_s [29]–[33]. However, it is necessary to previously normalize phase currents in order to make the method insensitive to load variations. Otherwise the variable-current amplitudes found in variable-speed drives would make the setting of the threshold impossible. The normalization in [29] and [30] is done using the modulus of the Park vector as follows:

$$i_{phN} = \frac{i_{ph}}{\sqrt{i_{ds}^2 + i_{qs}^2}} \tag{5}$$

where i_{ph} is the phase current and i_{phN} is the normalized phase current using the modulus of the Park vector.

Once normalized, the absolute value of i_{phN} is then averaged over the fundamental period

$$|i_{phN}(t)| = \frac{1}{T_s}\int_{t-T_s}^{t} |i_{phN}(t)|\, dt. \tag{6}$$

In prefault steady-state condition, the averaged absolute value of the phase currents is constant [29]

$$\xi = |i_{phN}|_{\text{pre}} = \frac{1}{\pi}\sqrt{\frac{8}{3}} \tag{7}$$

and then the fault detection index in [29] and [30] is defined as

$$e_k = \xi - |i_{phN}| \tag{8}$$

which is zero in healthy steady-state condition ($|i_{phN}| = |i_{phN}|_{pre} = \xi$) for all phases because the stator currents form a balanced electrical system.

After the OPF occurrence, the current in the faulty phase drops to zero and e_k converges to ξ after a fundamental period T_s (see Fig. 3). Assuming that a_1 is the faulty phase, it follows that

$$|i_{phN}|_{\text{post}} = 0 \ \text{ and } \ e_k = \xi, \ \text{for } k = a_1. \tag{9}$$

Consequently, the phase-current-based fault detection method (termed PHCFD in what follows) is based on monitoring e_k for all phases (i.e., $k \in \{a_1,\ b_1,\ c_1,\ a_2,\ b_2,\ c_2\}$ for the six-phase machine shown in Fig. 1), and defining a threshold in between zero and ξ ($0 \le T_{th} \le \xi$).

In an ideal scenario, the value of the fault index e_k for the remaining healthy phases would remain at zero after the fault occurrence. Unfortunately, the set of postfault currents is no longer balanced and the unequal values of the phase currents imply that

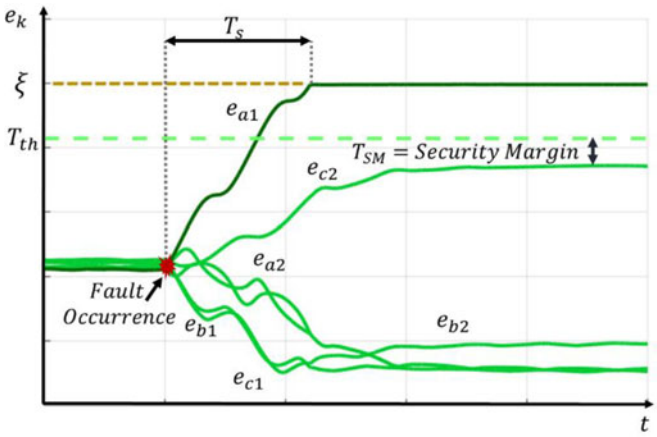

Fig. 3. Evolution of e_{ph} after the fault occurrence for phase a_1 (faulted) and phases $b_1,\ c_1,\ a_2,\ b_2$, and c_2 (healthy). Experimental results.

$$|i_{phN}|_{\text{post}} \neq \xi \ \text{ and } \ e_k \neq 0, \ \text{for } k \in \{b_1,\ c_1,\ a_2,\ b_2,\ c_2\}. \tag{10}$$

Even though $|e_k| \le \xi$ for the remaining healthy phases, the fact that these indices evolve to both positive and negative values diminishes to some extent the margin for the setting of the threshold T_{th}. For the sake of example, the threshold in Fig. 3 needs to be set above the postfault steady-state value of the index e_{c2} with a certain security margin (T_{SM}) that can be defined as a portion of the final value ξ

$$T_{\text{SM}} = \gamma \cdot \xi \tag{11}$$

where γ is the per unit vale of the security margin.

The threshold can then be set above the maximum value of the fault indices in the healthy phases (which is equal to $e_{c2}(\infty)$ in the example shown in Fig. 3)

$$T_{th} = e_k^{\max} + T_{\text{SM}} = e_{c2}(\infty) + T_{\text{SM}}. \tag{12}$$

It is also worth noting that the sinusoidal nature of the phase currents forces the integration (6) in a minimum time of one fundamental period (as shown in Fig. 3). Otherwise the integration in (6) would not provide the constant value ξ that is shown in (7). The speed of the detection method is, thus, limited by two factors: 1) the integration time cannot be set arbitrarily below T_s and 2) the threshold cannot be set below $e_{c2}(\infty)$.

Another practical issue is the determination of the fundamental period T_s and the implications of an erroneous estimation. If the drive is regulated with FOC, the fundamental period can be obtained from the control scheme as

$$\hat{T}_s = \frac{2\pi}{\hat{\omega}_s} \ \text{ with } \ \hat{\omega}_s = \frac{i_{qs}^*}{\tau_r \cdot i_{ds}^*} + p\omega_m \tag{13}$$

where $\tau_r = L_r/R_r$ is the rotor time constant, i_{ds}^* and i_{qs}^* are the *d-q* current references taken from the control. The calculation (13) implies no further computational cost since it is already done for the Park transformation in (2), but it is parameter dependent. Since the rotor time constant is known to vary at

different operating conditions, it can be concluded that, in general, $\hat{T}_s \neq T_s$. If $\hat{T}_s \neq T_s$, then $|i_{phN}|$ in (6) will not be equal to ξ in prefault condition. Furthermore, the moving average in the period $\hat{T}_s - T_s$ will make the fault detection index e_k to be sinusoidal at twice the fundamental frequency in prefault situation. If the error in the estimation $\hat{T}_s - T_s$ is reasonably low, the amplitude of this sinewave will remain below the threshold T_{th} and will not provoke false alarms. It is in any case an undesirable feature of the PHCFD technique.

Equations (6)–(9) directly express the method in [29] and [30] for three-phase machines. It has been, however, indicated in Section II that multiphase machines provide additional subspaces after the Clarke transformation compared to three-phase systems. For this reason, it seems natural to include these secondary components in the normalization of (5). In this way, following a similar procedure as in [33] (5) can be expressed as

$$i_{phN} = \frac{i_{ph}}{\sqrt{i_{ds}^2 + i_{qs}^2 + i_{xs}^2 + i_{ys}^2}}. \tag{14}$$

In prefault situation, $i_{xs} = i_{ys} = 0$, and, consequently, the result of (5) and (14) is the same, but after the OPF occurrence, both normalizations will provide a different evolution of the fault indices in the healthy phases. It must be noted, however, that the experimental comparison of the methods using (5) and (14), not shown in this manuscript for the sake of brevity, provides a similar performance and for this reason they are both simply referred as PHCFD.

To sum up, even though the phase-current-based method of [29], [30] can be extended using the normalization in (14), it still has the following shortcomings.

S1) The postfault values of the fault indices e_k in the healthy phases are nonnull. The unbalanced operation after the fault occurrence leads to both positive and negative values of all fault indices, and this diminishes the margin to select the threshold T_{th} in (12).

S2) The moving average is calculated using one fundamental period, and this implies that the fault index will need at least a time T_s to reach the value ξ (see Fig. 3). Although the selection of a proper threshold allows fault detection delays below T_s, this requirement slows down the speed of the fault detection.

S3) The prefault values of the fault indices e_k are only null if the estimated period of the fundamental component ($\hat{T}_s$) is equal to the actual period T_s. Since $\hat{T}_s$ is typically estimated using (13), this makes the method parameter dependent to some extent.

Aiming to overcome these limitations, the next section suggests a VSDFD method with the capability to maintain postfault healthy indices close to zero, calculating the moving average in a window below T_s and obtaining prefault indices that are insensitive to the estimated period $\hat{T}_s$.

IV. Proposed Open-Phase Fault Detection Method for Six-Phase Induction Motor Drives

Even though multiphase machines offer additional planes after the VSD, most of the existing OPF detection methods still follow a phase-current approach that is essentially similar to the three-phase case because they are developed in a per-phase basis [26]–[28], [33]. On the contrary, the indices suggested in this study are based on the VSD variables and overcome the aforementioned limitations S1 to S3.

From the generalized Clarke transformation (1) and setting the OPF condition ($i_{ph} = 0$), it is possible to express the OPF restriction as the ratio of VSD variables. For the sake of example, if the OPF occurs in phase a_1, the condition $i_{a1} = 0$ provides the physical restriction $-\frac{i_x}{i_\alpha} = 1$ from the first row in (1) after inversing the Clarke matrix. By defining the ratio $R_{a1} = -\frac{i_x}{i_\alpha}$, it follows that R_{a1} is forced to be one after the fault by the physical OPF condition. Since $i_x^* = 0$ before the fault and the current controllers ensure a good current tracking of the $x-y$ currents, the ratio R_{a1} is close to zero in prefault situation. The OPF condition together with the null prefault $x-y$ currents ensure that the ratio R_{a1} is close to zero in prefault situation and one after the fault occurs. Consequently, the ratio R_{a1} provides a simple mean to identify the fault occurrence in phase a_1 with well-established values in pre- and postfault situations. Proceeding in the same manner, it is possible to define similar ratios for the other phases

$$\begin{aligned}
R_{a1} &= -\frac{i_x}{i_\alpha}, \quad R_{b1} = \frac{i_x}{-i_\alpha + \sqrt{3}\cdot i_\beta - \sqrt{3}\cdot i_y}, \\
R_{c1} &= \frac{i_x}{-i_\alpha - \sqrt{3}\cdot i_\beta + \sqrt{3}\cdot i_y} \\
R_{a2} &= \frac{i_x}{i_\alpha + \frac{1}{\sqrt{3}} i_\beta + \frac{1}{\sqrt{3}} i_y}, \quad R_{b2} = \frac{i_x}{i_\alpha - \frac{1}{\sqrt{3}} i_\beta - \frac{1}{\sqrt{3}} i_y}, \\
R_{c2} &= -\frac{i_y}{i_\beta}.
\end{aligned} \tag{15}$$

The ratios R_k in (15) are already normalized and they are zero and unity before and after the OPF occurrence, respectively. Compared to the sinewaves that result from the normalized phase currents i_{phN} in (5) or (14), the ratios R_k in (15) are constantly zero at any instant in prefault situation. This in turn implies that while phase currents need to be averaged over a fundamental period in (6) to obtain the constant value ξ, the ratios $R_k = 0\ \forall t$. Consequently, the limitation S3 is directly avoided because the periods of the moving average T_m and the estimated value $\hat{T}_s$ have no impact on the averaged ratios R_k.

Similarly to the PHCFD approach, the ratios R_k can be integrated using a moving average

$$\langle\, R_k(t) \,\rangle = \frac{1}{T_m} \int_0^{T_m} R_k(t)\, dt \tag{16}$$

but opposite to (6), it is not necessary to calculate the absolute value and the period of the moving average T_m does not need to coincide with the fundamental period T_s. On the contrary, the period T_m can be freely chosen as a certain portion of $\hat{T}_s$

$$T_m = \sigma \cdot \hat{T}_s\ , \quad \sigma \leq 1 \tag{17}$$

where σ is a parameter that defines the portion of the fundamental period that is used in the moving average. The selection of σ is a tradeoff between the fault indices noise and the OPF

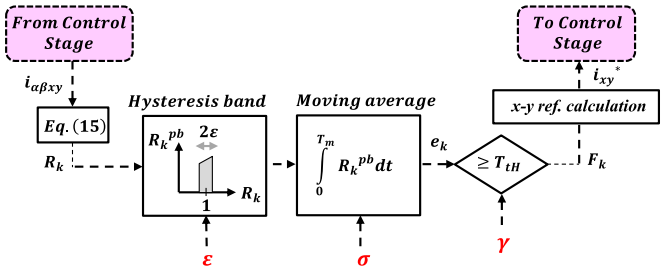

Fig. 4. Proposed fault detection scheme VSDFD (see Fig. 2 to link with the control scheme).

detection speed. Setting a value $\sigma = 1$ as in the PHCFD approach may results in longer detection times, whereas values of σ too close to zero will unacceptably increase the fault indices ripple. Further details on the selection of σ will be provided in Section V, but in any case the freedom to choose a value of $\sigma \leq 1$ also eliminates the limitation S2.

Finally, the limitation S1 is eliminated by applying a hysteresis band to the ratios R_k for noise rejection. Since it is known that only the faulty ratio will be constantly 1 after the OPF occurrence, all indices are filtered using the following hysteresis band:

$$\begin{aligned} &\text{if} \quad 1-\varepsilon \leq R_k \leq 1+\varepsilon, \quad \text{then} \quad R_k^{pb} = R_k \\ &\text{else} \quad R_k^{pb} = 0 \end{aligned} \tag{18}$$

where ε is the width of the hysteresis band in (18). This width should be limited in order to ensure a low ripple of the fault indices of the healthy phases. A 10% of the postfault index value (i.e., $\varepsilon = 0.1$) typically provides a sufficient security margin, but it is also possible to increase the value of σ if the current ripple is higher in order to limit the oscillations (see Section V).

If the filtered values R_k^{pb} are then averaged as in (16), the new fault indices are

$$e_k = \int_{t-T_m}^{t} R_k^{pb}(t)dt, \quad k \in \{a_1,\ b_1,\ c_1,\ a_2,\ b_2,\ c_2\}. \tag{19}$$

Finally, the information of the faulty phases F_k is obtained comparing the fault indices with the threshold

$$\begin{aligned} &\text{if } e_k \geq T_{th}, \quad \text{then} \quad F_k = 1 \\ &\text{else} \quad F_k = 0. \end{aligned} \tag{20}$$

At this stage, the OPF has been detected and localized, but it is still necessary to calculate the *x*-*y* current references. According to a certain criteria, such as minimum loss (ML) or maximum torque (MT), the fault detection scheme provides the references that serve as an input for the *x*-*y* Proportiona Resonant controller (see Fig. 2). The previously described steps (15)–(20) are summarized in the fault detection scheme of Fig. 4. The calculation of the faulty state F_k is simple: the calculation of R_k just implies few arithmetic operations, and then it is just necessary to filter using a hysteresis band and integrate over the period T_m. In addition to the simplicity, the method overcomes limitations S1 to S3. The goodness of the proposed VSDFD method is experimentally evaluated in the next section to verify its speed of detection and robustness.

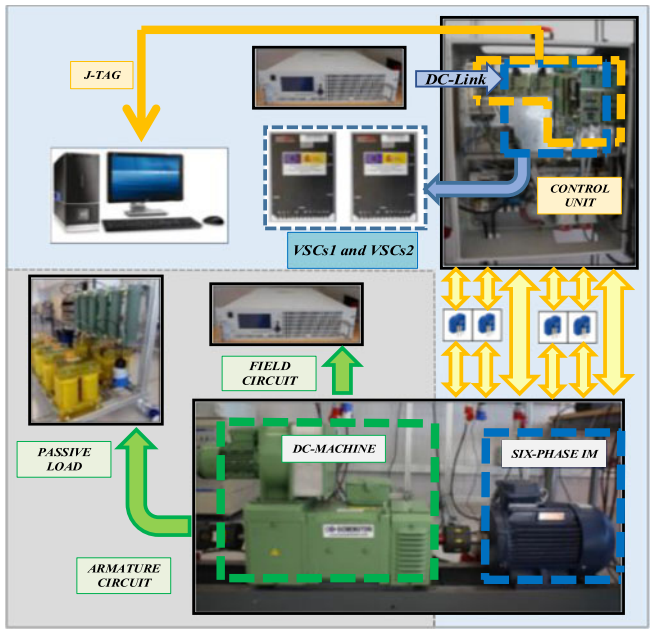

Fig. 5. Scheme of the test bench used for the experimental results.

TABLE I
RATED VALUES OF THE MOTOR

Power (kW)	1.4
I_{peak} (A)	5
i_d (A)	1.4
i_q (A)	8.5
n_m (r/min)	1000
T_{load} (N·m)	13.4

V. EXPERIMENTAL RESULTS

A. Experimental Rig

A scheme of the experimental system used for the analysis is shown in Fig. 5. The system consists of an asymmetrical six-phase IM driven by two conventional two-level three-phase VSCs from Semikron (SKS22F modules) that are controlled using the scheme shown in Fig. 2. The parameters of the custom-built multiphase machine have been determined using ac-time domain and standstill with inverter supply tests [40], [41]. The obtained parameters are: stator and rotor resistances of 4.2 and 2 Ω, stator and rotor leakage inductances of 4.2 and 55 mH, and mutual inductance of 420 mH. The rated values of the six-phase IM are included in Table I.

The VSCs are connected to a single dc power supply and the control actions are performed by a digital signal processor (TMS320F28335 from Texas Instruments, TI). The control unit is programmed using a JTAG and the TI proprietary software called Code Composer Studio. Four hall-effect sensors (LEM LAH 25-NP) and a digital encoder (GHM510296R/2500) have been used to obtain the current and speed measurements, respectively. The six-phase IM is loaded by a dc machine that is coupled to the shaft and whose armatures are connected to a variable passive *R* load that dissipates the power. The load torque is consequently speed dependent.

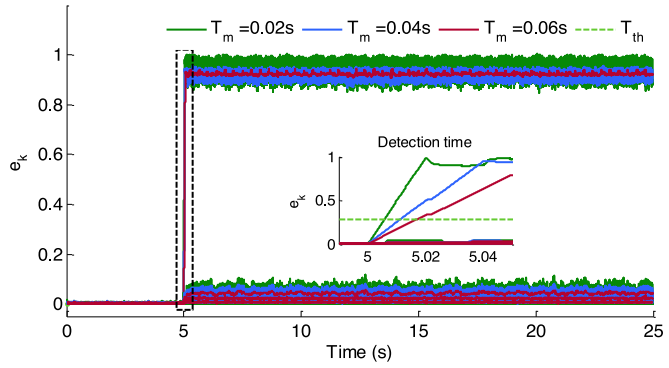

Fig. 6. Evolution of the fault detection indices e_k in the proposed VSDFD method in single OPF for different periods T_m . $\sigma = 1$ (red), $\sigma = 0.66$ (blue), and $\sigma = 0.33$ (green).

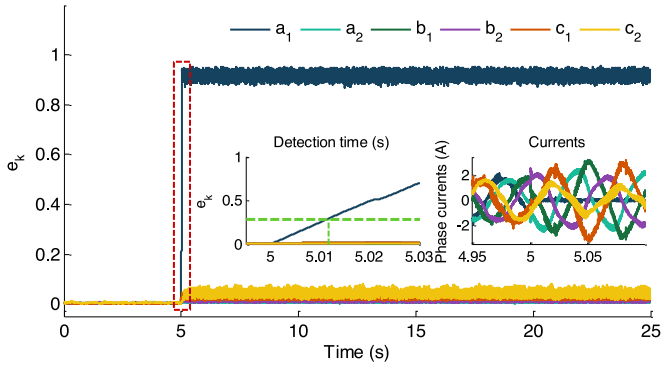

Fig. 7. *Test 1:* Evolution of the fault detection indices (e_k) in the proposed method VSDFD in the event of a single OPF at $t = 5$ s.

B. Experimental Results

Before proceeding to show some tests, it is first necessary to set parameters γ, ε, and σ that define the proposed VSDFD method in Fig. 4.

1) *Security margin*: The value of γ in (11) is set to 0.1, thus resulting in a threshold $T_{th} = 0.2862$ which has a security margin $T_{\mathrm{SM}} = 0.1$ above the maximum postfault value of the healthy phases: $e_k^{\max} = 0.188$.
2) *Hysteresis band width*: The value of ε in (18) is set to 0.1, obtaining a hysteresis band for $R_k^{pb} \in [0.9, 1.1]$.
3) *Period of the moving average*: The selection of σ in (17) requires some attention. While decreasing the value of T_m accelerates the rise of the faulty phase index after the fault occurrence, an excessively low value of σ will also increase the ripple of the fault indices e_k. Fig. 6 shows the experimental results of the indices e_k for three values of σ (1, 0.66, and 0.33) with $T_s = 0.06$ s. In all three cases, the index of the faulty phase rises after the OPF occurs at $t = 5$ s, whereas the indices of the healthy phases remain close to zero. It can be noted, however, that the rising slope is larger for lower values of σ (red trace in Fig. 6) at the expense of an increased ripple. Conversely, setting $\sigma = 1$ as in the PHCFD method reduces the ripple but leads to longer detection times (red trace in Fig. 6). The value of σ is set to 0.66, in this paper to obtain a high speed of detection without increasing the ripple in excess.

Once the VSDFD method is defined, test 1 for single OPF is shown in Fig. 7, where phase a_1 is opened at $t = 5$ s. In this test, the machine is operated with $i_d^* = 1.1$ A at 300 r/min and 3.2 N·m. In the zoom-in right plot of Fig. 7, it can be noted that the currents become unbalanced after the fault occurrence, this causing the appearance of nonnull x-y currents. As a consequence, the fault index of phase a_1 quickly rises while the rest of indices remain close to zero. The detection time is 11.7 ms which is about 18% of the fundamental period. This low detection time is possible due to two main causes: 1) the slope of the faulty index is high because $\sigma \leq 1$ and 2) the threshold is low because $e_k^{\max}$ is also low. If higher detection times are admissible, it is possible to increase the security margin and elevate the threshold at the expense of longer detection times. On the other hand, the detection time can be further reduced setting lower values of σ at the expense of higher ripple in the fault indices. Both the quick rise of the faulty index and the high margin to set the threshold are key features of the proposed VDFD method.

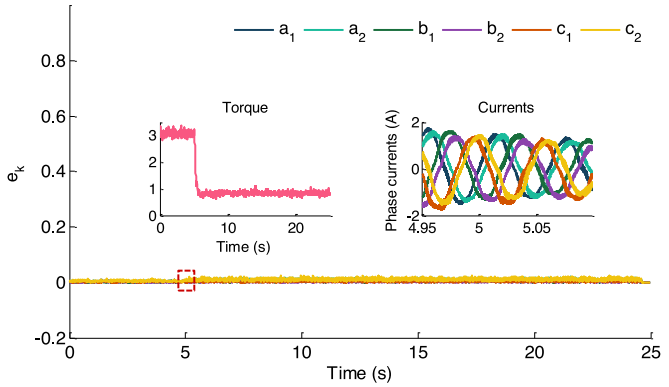

Fig. 8. *Test 2:* Evolution of the fault detection indices (e_k) in the proposed method VSDFD in the event of a step in the load torque at $t = 5$ s.

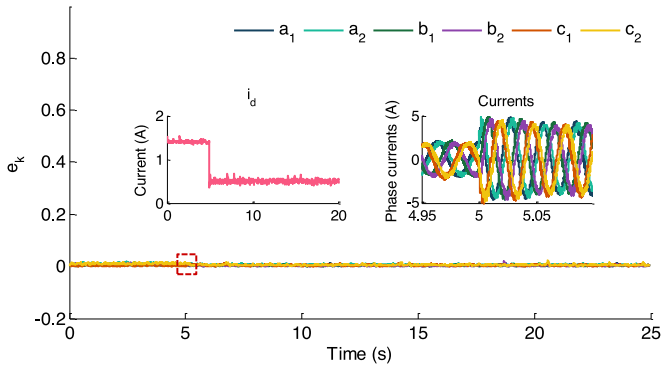

Fig. 9. *Test 3:* Evolution of the fault detection indices (e_k) in the proposed method VSDFD in the event of a step in the d-current at $t = 5$ s.

Apart from the detection speed, it is also necessary to prove that the VSDFD method is robust against transients, avoiding false alarms. For this purpose, three tests have been performed: test 2, where the machine is unloaded from 3 to 1 N·m at $t = 5$ s (see Fig. 8), test 3, where the reference of the d-current is stepped from 1.2 to 0.4 A (see Fig. 9), and test 4, where the speed reference is varied from 300 to 500 r/min at $t = 5$

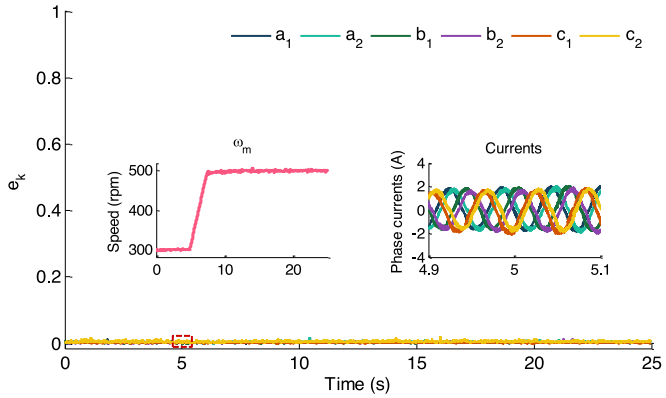

Fig. 10. *Test 4:* Evolution of the fault detection indices (e_k) in the proposed method VSDFD in the event of a speed ramp at $t = 5$ s.

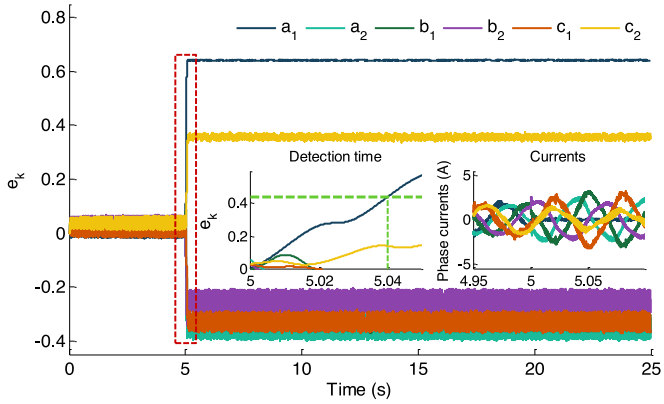

Fig. 12. *Test 1:* Evolution of the fault detection indices (e_k) in the benchmark method PHCFD in the event of a single OPF at $t = 5$ s.

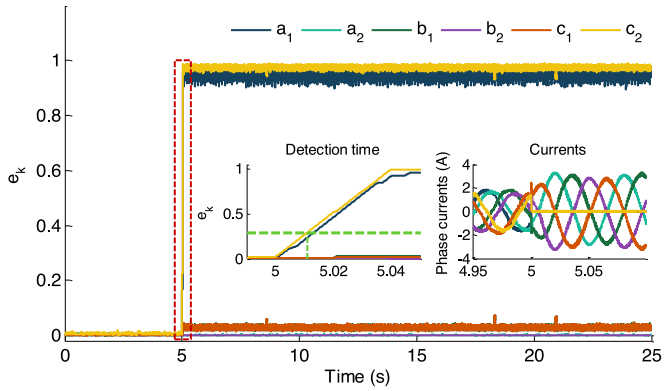

Fig. 11. *Test 5:* Evolution of the fault detection indices (e_k) in the proposed method VSDFD in the event of two OPFs at $t = 5$ s.

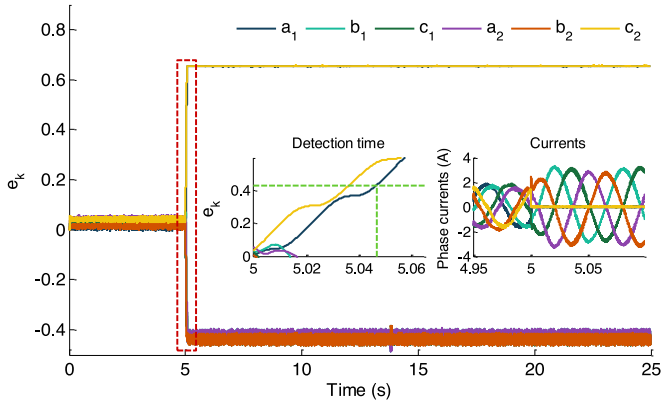

Fig. 13. *Test 5:* Evolution of the fault detection indices (e_k) in the benchmark method PHCFD in the event of two OPFs at $t = 5$ s.

s (see Fig. 10). The changes in the torque/flux/speed of tests 2/3/4 force a transient in the machine, whose stator current is decreased/increased/increased for $t \geq 5$ s (see the right zoom-in plots in Figs. 8–10). In spite of the sudden steps of torque/flux and the speed ramp, (3) shows that the flux and torque modifications only affect the $\alpha - \beta$ subspace. Consequently, the x-y currents remain regulated to zero by the inner current loop of Fig. 2 regardless of the dynamics conditions [2], and this implies that the ratios in (15) are also kept at zero mean value with a small ripple. The fault indices e_k in Figs. 8–10 prove to be completely unaffected by the torque/flux/speed transients. The decoupling of the orthogonal x-y plane provides a good robustness to the VSDFD method against any kind of transient in prefault operation.

The verification of multiple OPFs is finally verified in test 5, where phases a_1 and c_2 are opened at approximately $t = 5$ s. Due to some delay in the relays that perform the OPF, the instant when the two phases are opened is slightly displaced in time around 1 ms, as it can be appreciated in the left zoom-in plot of Fig. 11. Similarly to test 1, the indices of the faulty phases rapidly rise after the fault occurrence, whereas the healthy indices stay at values close to zero. The detection time is again around 10 ms which is 16% of the fundamental period. Test 5 confirms that multiple OPFs can be detected with similar speed of detection as in the single OPF scenario. The machine operating conditions in this test are the same as in test 1.

All in all, tests 1–5 of Figs. 7–11 confirm the capability of the proposed VSDFD method to detect single and multiple OPFs with a detection speed around 17% of the fundamental period and good robustness. This satisfactory performance is obtained with a simple procedure and satisfies requirements R1 to R5 shown in the introduction.

In order to compare the performance of the VSDFD method with the phase current-based approach from [29], [30], the PHCFD performance is evaluated in the same tests 1 and 5 used for VSDFD in Figs. 7–11. Aiming to do a fair comparison, the security margin is also set as $\gamma = 0.1$. However, since the fault indices do not remain close to zero after the fault in PHCFD, the value of $e_k^{\max}$ is increased up to 0.33 (see e_{c2} in Fig. 12), which elevates the threshold to a value $T_{th} = 0.43$. On the other hand, the moving average period T_m is mandatorily equal to the estimated fundamental period $\hat{T}_s$.

Under the same conditions and equivalent parameters, the results for PHCFD are shown in Figs. 12 and 13 for the cases of single (phase a_1) and dual (phases a_1 and c_2) OPFs. As it can be observed from Fig. 12, the detection time is around 40 ms, which is 66% of the fundamental period. Compared to Fig. 7, the proposed VSDFD method is nearly four times faster than

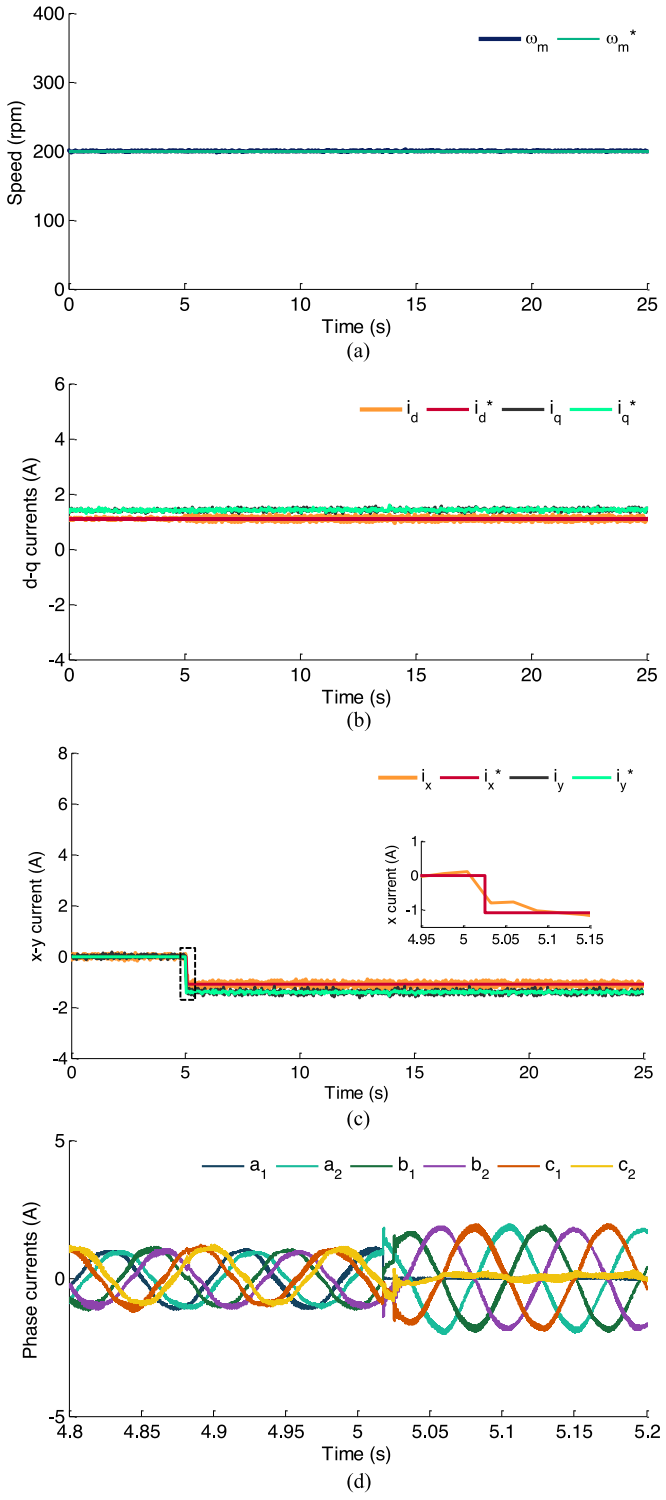

Fig. 14. *Test 6:* Transition from pre- to postfault situation under a_1 OPF. From top to bottom: (a) Motor speed, (b) *d-q* currents, (c) x-y currents, and (d) phase currents.

the benchmark PHCFD technique. The slower behavior of the PHCFD is caused by a longer moving average period and a higher threshold. The case with two OPFs using PHCFD is finally shown in Fig. 13. In this case, all healthy indices become negative after the OPF occurrence, and this reduces the $e_k^{\max}$ value. According to (12), this means that it is also possible to reduce the threshold T_{th} value for this specific fault. Nevertheless, it is not possible to set the value of T_{th} *a posteriori* once the information about the type of fault is available. Consequently, the threshold must be set in advance considering the most unfavorable scenario, and for this reason, T_{th} is maintained at 0.43 as in test 1. The PHCFD proves to correctly detect and localize the OPFs in the faulty phases a_1 and c_2 with a detection delay around 66% of the fundamental period (46 ms). Compared to Fig. 11, it is verified again that in the event of multiple OPFs, the proposed VSDFD method is much faster (nearly four times) than the benchmark PHCFD technique.

TABLE II
VALUES OF SYNCHRONOUS AND ANTISYNCHRONOUS CONTROLLERS

Controller	PI ω	PI d current	PI q current	PI x current	PI y current
K_p	0.75	50	120	22	22
K_i	0.45	5	35	100	100

Finally, the transition from pre- to postfault situation is tested under a_1 OPF situation (test 6). The VSDFD method is integrated in the control scheme of the Fig. 2. The phase a_1 is opened at $t = 5.015$ s, and, therefore, the current cannot flow through this phase (see Fig 14(d)). The VSDFD method detects the fault in approximately 10 ms and then the x-y reference currents are properly modified according to the maximum torque mode [42], as it is shown in the Fig. 14(c). Moreover, when the OPF occurs in phase a_1 , the x-y reference currents in maximum torque mode are inversely proportional to α-β and a rotation in the forward (synchronous) direction using Park transformation (2) provides constant x-y references [43]. For this reason, this rotation is applied to x-y components after the fault is detected. The OPF detection time is so short that the speed regulation is not affected by the fault, confirming the smooth transition from pre- to postfault modes of operation (see Fig. 14(a)). Fig. 14(b) finally shows that d-q currents remain unaffected after the OPF occurrence. Table II shows the gains of the controllers used in the tests, which have been adjusted to obtain a satisfactory performance both in terms of overshooting and rising time.

The integration of the fault detection technique together with the fault-tolerant control whose results are shown in Fig. 14 proves the capability of the six-phase drive to self-reconfigure the control in the software stage and provides enhanced reliability without additional hardware.

VI. CONCLUSION

Fault detection techniques in electrical drives are key issues in industry applications where reliability is a main concern. Most of the fault detection methods are based on fault indices that are elaborated from preprocessed phase currents. In the specific case of multiphase machines, it is, however, possible to follow a VSD approach to formulate these fault indices. Using normalized *x-y* currents together with a hysteresis band, the OPFs can be detected and localized with good robustness and detection speeds nearly four times faster than applying conventional

phase-current-based methods. In addition, the calculation of the moving average based on constant (zero) currents, the exclusion of the *x-y* plane in the torque/flux production, the possibility to use an arbitrary period for the moving average window, and the capability to maintain the indices of the healthy phases close to zero after the fault are key features of the proposed method.

Since the purpose of the proposed fault detection method is to be integrated into a fault-tolerant control, the VSD approach for the fault detection can naturally be inserted into conventional VSD-based control strategies. The suggested technique can be used in conjunction with high-performance fault-tolerant control methods for six-phase variable-speed drives without the requirement of additional hardware and with independence of the operating point, the type of control, and the electrical and mechanical parameters. Simplicity is then preserved and fast detection times are guaranteed as well as a smooth transition from pre- to postfault states of the drive.

Although the method developed in this study is specifically designed for six-phase drives, it can be easily generalized to any distributed-winding multiphase machine with a proper redefinition of the fault indices.

REFERENCES

[1] E. Levi, "Advances in converter control and innovative exploitation of additional degrees of freedom for multiphase machines," *IEEE Trans. Ind. Electron.*, vol. 63, no. 1, pp. 433–448, Jan. 2016.

[2] F. Barrero and M. J. Duran, "Recent advances in the design, modeling and control of multiphase machines—Part 1," *IEEE Trans. Ind. Electron.*, vol. 63, no. 1, pp. 449–458, Jan. 2016.

[3] M. J. Duran and F. Barrero, "Recent advances in the design, modeling and control of multiphase machines—Part 2," *IEEE Trans. Ind. Electron.*, vol. 63, no. 1, pp. 459–468, Jan. 2016.

[4] A. Cavagnino, Z. Li, A. Tenconi, and S. Vaschetto, "Integrated generator for more electric engine: Design and testing of a scaled-size prototype," *IEEE Trans. Ind. Appl.*, vol. 49, no. 5, pp. 2034–2043, Sep./Oct. 2013.

[5] G. Sulligoi, A. Tessarolo, V. Benucci, A. M. Trpani, M. Baret, and F. Luise, "Shipboard power generation: Design and development of a medium-voltage dc generation system," *IEEE Ind. Appl. Mag.*, vol. 19, no. 4, pp. 47–55, Jul. 2013.

[6] E. Jung, H. Yoo, S. Sul, H. Choi, and Y. Choi, "A nine-phase permanent-magnet motor drive system for an ultrahigh-speed elevator," *IEEE Trans. Ind. Appl.*, vol. 48, no. 3, pp. 987–995, May/Jun. 2012.

[7] H. S. Che, E. Levi, M. Jones, M. J. Duran, W. P. Hew, and N. A. Rahim, "Operation of a six-phase induction machine using series-connected machine-side converters," *IEEE Trans. Ind. Electron.*, vol. 61, no. 1, pp. 164–176, Jan. 2014.

[8] (2016, Oct. 25). *Gamesa Technological Corporation S. A.Gamesa 5.0 MW*. [Online]. Available: http://www.gamesacorp.com/recursos/doc/productos-servicios/aerogeneradores/catalogo-g10x-45mw.pdf

[9] H. S. Che *et al.*, "Post-fault operation of an asymmetrical six-phase induction machine with single and two isolated neutral points," *IEEE Trans. Power Electron.*, vol. 29, no. 10, pp. 5406–5416, Oct. 2014.

[10] I. Gonzalez-Prieto, M. J. Duran, F. Barrero, M. Bermudez, and H. Guzman, "Impact of post-fault flux adaptation on six-phase induction motor drives with parallel converters," *IEEE Trans. Power Electron.*, vol. 32, no. 1, pp. 515–528, Jan. 2017.

[11] A. Tani, M. Mengoni, L. Zarri, G. Serra, and D. Casadei, "Control of multiphase induction motors with an odd number of phases under open-circuit phase faults," *IEEE Trans. Power Electron.*, vol. 27, no. 2, pp. 565–577, Feb. 2012.

[12] R. Kianinezhad, B. Nahid-Mobarakeh, L. Baghli, F. Betin, and G. A. Capolino, "Modeling and control of six-phase symmetrical induction machine under fault condition due to open phases," *IEEE Trans. Ind. Electron.*, vol. 55, no. 5, pp. 1996–1977, May 2008.

[13] A. Mohammadpour and L. Parsa, "Global fault-tolerant control technique for multi-phase permanent-magnet machines," *IEEE Trans. Ind. Appl.*, vol. 51, no. 1, pp. 178–186, Jan./Feb. 2015.

[14] A. S. Abdel-Khalik, A. S. Morsy, S. Ahmed, and A. M. Massoud, "Effect of stator winding connection on performance of five-phase induction machines," *IEEE Trans. Ind. Electron.*, vol. 61, no. 1, pp. 3–19, Jan. 2014.

[15] M. Bermudez, I. Gonzalez-Prieto, F. Barrero, H. Guzman, M. J. Duran, and X. Kestelyn, "Open-phase fault-tolerant direct torque control technique for five-phase induction motor drives," *IEEE Trans. Ind. Electron.*, vol. 64, no. 2, pp. 902–911, Feb. 2017.

[16] H. Guzmán, M. J. Duran, F. Barrero, B. Bogado, and S. Toral, "Speed control of five-phase induction motors with integrated open-phase fault operation using model-based predictive current control techniques," *IEEE Trans. Ind. Electron.*, vol. 61, no. 9, pp. 4474–4484, Sep. 2014.

[17] H. Guzman *et al.*, "Comparative study of predictive and resonant controllers in fault-tolerant five-phase induction motor drives," *IEEE Trans. Ind. Electron.*, vol. 63, no. 1, pp. 606–617, Jan. 2016.

[18] F. Betin and G. A. Capolino, "Shaft positioning for six-phase induction machines with open phases using variable structure control," *IEEE Trans. Ind. Electron.*, vol. 59, no. 6, pp. 2612–2620, Jun. 2012.

[19] H. Henao *et al.*, "Trends in fault diagnosis for electrical machines: A review of diagnostic techniques," *IEEE Ind. Electron Mag.*, vol. 8, no. 2, pp. 31–42, Jun. 2014.

[20] M. Riera-Guasp, J. A. Antonino-Daviu, and G. A. Capolino, "Advances in electrical machine, power electronic, and drive condition monitoring and fault detection: State of the art," *IEEE Trans. Ind. Electron.*, vol. 62, no. 3, pp. 1746–1759, Mar. 2015.

[21] A. Kontarcek, P. Bajec, M. Nemec, V. Ambrozic, and D. Nedeljkovic, "Cost-effective three-phase PMSM drive tolerant to open-phase fault," *IEEE Trans. Ind. Electron.*, vol. 62, no. 11, pp. 6708–6718, Nov. 2015.

[22] J. Hang, J. Zhang, M. Cheng, and S. Ding, "Detection and discrimination of open-phase fault in permanent magnet synchronous motor drive system," *IEEE Trans. Power Electron.*, vol. 31, no. 7, pp. 4697–4709, Jul. 2016.

[23] L. Zarri *et al.*, "Detection and localization of stator resistance dissymmetry based on multiple reference frame controllers in multiphase induction motor drives," *IEEE Trans. Ind. Electron.*, vol. 60, no. 8, pp. 3506–3518, Aug. 2013.

[24] F. Immovilli, C. Bianchini, E. Lorenzani, A. Bellini, and E. Fornasiero, "Evaluation of combined reference frame transformation for interturn fault detection in permanent-magnet multiphase machines," *IEEE Trans. Ind. Electron.*, vol. 62, no. 3, pp. 1912–1920, Mar. 2015.

[25] B. Sen and J. Wang, "Stator interturn fault detection in permanent-magnet machines using PWM ripple current measurement," *IEEE Trans. Ind. Electron.*, vol. 63, no. 7, pp. 3148–3157, May 2016.

[26] M. Salehifar, R. S. Arashloo, M. Moreno-Eguilaz, V. Sala, and L. Romeral "Observer-based open transistor fault diagnosis and fault-tolerant control of five-phase permanent magnet motor drive for application in electric vehicles," *IET Power Electron.*, vol. 8, no. 1, pp. 76–87, 2015.

[27] S. Mehdi, M. Moreno-Eguilaz, G. Putrus, and P. Barras, "Simplified fault tolerant finite control set model predictive control OFA five-phase inverter supplying BLDC motor in electric vehicle drive," *Elsevier Electr. Power Syst. Res.*, vol. 132, pp. 56–66, 2016.

[28] M. Taherzadeh, S. Carriere, F. Betin, M. Joorabian, R. Kianinezhad, and G. A. Capolino, "A novel strategy for sensorless control modification of a six-phase induction generator in faulted mode," *Electr. Power Compon. Syst.*, vol. 44, no. 8, pp. 941–953, 2016.

[29] J. O. Estima and A. J. M. Cardoso, "A new approach for real-time multiple open-circuit fault diagnosis in voltage source inverters," *IEEE Trans. Ind. Appl.*, vol. 47, no. 6, pp. 2487–2494, Nov./Dec. 2011.

[30] N. M. A. Freire, J. O. Estima, and A. J. M. Cardoso, "Open-circuit fault diagnosis in PMSG drives for wind turbine applications," *IEEE Trans. Ind. Electron.*, vol. 60, no. 9, pp. 3957–3967, Sep. 2013.

[31] W. Sleszynski, J. Nieznanski, and A. Cichowski, "Open-transistor fault diagnostics in voltage source inverters by analyzing the load currents," *IEEE Trans. Ind. Electron.*, vol. 56, no. 11, pp. 4681–4688, Nov. 2009.

[32] J. O. Estima and A. J. M. Cardoso, "A new algorithm for real-time multiple open-circuit fault diagnosis in voltage-fed PWM motor drives by the reference current errors," *IEEE Trans. Ind. Electron.*, vol. 60, no. 8, pp. 3496–3505, Aug. 2013.

[33] M. Trabelsi, N. K. Nguyen, and E. Semail, "Real-time switches fault diagnosis based on typical operating characteristics of five-phase permanent-magnetic synchronous machines," *IEEE Trans. Ind. Electron.*, vol. 63, no. 8, pp. 4683–4694, Aug. 2016.

[34] S. K. Baek, H. U. Shin, S. Y. Kang, C. S. Park, and K. B. Lee, "Open fault detection and tolerant control for a five phase inverter driving system," *Energies*, vol. 9, no. 5, pp. 355–374, 2016.

[35] H. U. Shin, S. K. Baek, and K. B. Lee, "Fault detection and fault-tolerant operation of a five-phase induction motor driving system," in *Proc. IEEE Power Electron. Motion Control Conf.*, 2016, pp. 2487–2492.
[36] F. Meinguet, E. Semail, and J. Gyselinck, "An on-line method for stator fault detection in multi-phase PMSM drives," in *Proc. IEEE Veh. Power Propulsion Conf.*, Lille, France, 2010, pp. 1–6.
[37] Y. Zhao and T. A. Lipo, "Space vector PWM control of dual three-phase induction machine using vector space decomposition," *IEEE Trans. Ind. Appl.*, vol. 31, no. 5, pp. 1100–1109, Sep./Oct. 1995.
[38] M. J. Duran, I. Gonzalez-Prieto, F. Barrero, M. Mengoni, L. Zarri, and E. Levi, "A simple braking method for six-phase induction motor drives with diode front-end rectifier," in *Proc. 2015 41st Annu. Conf. IEEE Ind. Electron. Soc.*, Nov. 9–12, 2015, pp. 001542–001547.
[39] I. Subotic, N. Bodo, E. Levi, M. Jones, and V. Levi, "Isolated chargers for EVs incorporating six-phase machines," *IEEE Trans. Ind. Electron.*, vol. 63, no. 1, pp. 653–664, Jan. 2016.
[40] A. Yepes *et al.*, "Parameter identification of multiphase induction machines with distributed windings—Part 1: Sinusoidal excitation methods," *IEEE Trans. Energy Convers.*, vol. 27, no. 4, pp. 1056–1066, Dec. 2012.
[41] J. A. Riveros *et al.*, "Parameter identification of multiphase induction machines with distributed windings—Part 2: Time-domain techniques," *IEEE Trans. Energy Convers.*, vol. 27, no. 4, pp. 1067–1077, Dec. 2012.
[42] W. N. W. A. Munim, M. J. Duran, H. S. Che, M. Bermudez, I. Gonzalez-Prieto, and N. A. Rahim, "A unified analysis of the fault tolerance capability in six-phase induction motor drive," *IEEE Trans. Power Electron.*, doi: 10.1109/TPEL.2016.2632118, *Early Access*, 2017.
[43] M. J. Duran, I. Gonzalez-Prieto, M. Bermudez, F. Barrero, H. Guzman, and M. R. Arahal, "Optimal fault-tolerant control of six-phase induction motor drives with parallel converters" *IEEE Trans. Ind. Electron.*, vol. 63, no. 1, pp. 629–640, Jan. 2016.

Mario J. Duran was born in Málaga, Spain, in 1975. He received the M.Sc. and Ph.D. degrees in electrical engineering from the University of Málaga, Málaga, in 1999 and 2003, respectively.

He is currently an Associate Professor in the Department of Electrical Engineering, University of Málaga. His research interests include modeling and control of multiphase drives and renewable energies conversion systems.

Ignacio Gonzalez-Prieto was born in Malaga, Spain, in 1987. He received the Industrial Engineer and M.Sc. degrees from the University of Malaga, Malaga, in 2012 and 2013, respectively, and the Ph.D. degree in automatic and electronic engineering from the University of Seville, Seville, Spain, in 2016.

He is currently a Researcher in the Department of Electrical Engineering, University of Malaga. His research interests include multiphase machines, fault detection methods, wind energy systems, and electrical vehicles.

Natalia Rios-Garcia was born in Malaga, Spain, in 1993. She received the Industrial Engineer degree from the University of Malaga, Malaga, in 2016, where she is currently working toward the M.Sc. degree.

Her research interests include multiphase machines, fault detection methods, wind energy systems, and electrical vehicles.

Federico Barrero (M'04–SM'05) received the M.Sc. and Ph.D. degrees in electrical and electronic engineering from the University of Seville, Seville, Spain, in 1992 and 1998, respectively.

In 1992, he joined the Department of Electronic Engineering, University of Seville, where he is currently a Full Professor.

Dr. Barrero received the Best Paper Awards from the IEEE TRANSACTIONS ON INDUSTRIAL ELECTRONICS for 2009 and from the IET Electric Power Applications for 2010–2011.